

## TURBULENT EROSION OF MAGNETIC FLUX TUBES

K. PETROVAY AND F. MORENO-INSERTIS

Instituto de Astrofísica de Canarias, 38200 La Laguna (Tenerife), Spain; kpetro@ll.iac.es, fmi@ll.iac.es

Received 1996 October 16; accepted 1997 March 13

### ABSTRACT

Results from a numerical and analytical investigation of the solution of a nonlinear axisymmetric diffusion equation for the magnetic field are presented for the case when the nonlinear dependence of the diffusivity  $\nu(B)$  on the magnetic field satisfies basic physical requirements. We find that for sufficiently strong nonlinearity (i.e., for sufficiently strong reduction of  $\nu$  inside the tube) a current sheet is spontaneously formed around the tube within one diffusion timescale. This sheet propagates inward with a velocity inversely proportional to the ratio of the field strength just inside the current sheet to the equipartition field strength  $B_0/B_e$ , so the lifetime of a tube with constant internal flux density is increased approximately by a factor not exceeding  $B_0/B_e$ , even for infinitely effective inhibition of turbulence inside the tube. Among the applications of these results, we point out that toroidal flux tubes in the solar convective zone are subject to significant flux loss owing to turbulent erosion on a timescale of  $\sim 1$  month and that turbulent erosion may be responsible for the formation of a current sheet around a sunspot. It is further proposed that, despite the simplifying assumptions involved, our solutions correctly reflect the essential features of the sunspot decay process.

*Subject headings:* magnetic fields — MHD — sunspots — turbulence

### 1. INTRODUCTION

The relation of turbulence to magnetic structures is ambivalent. On the one hand, any magnetic field concentration will tend to be smeared out by the process of turbulent diffusion due to smaller scale motions. Since first proposed by Sweet (1950), this process of *turbulent magnetic diffusion* characterized by a diffusivity  $\nu \sim lv$  (where  $l$  is the scale of the turbulence and  $v$  is its r.m.s. velocity) was and, despite repeated controversies, has remained a cornerstone of mean field magnetohydrodynamics, observable, e.g., in the form of a slow dissolution of unipolar areas on the solar surface (Sheeley, DeVore, & Boris 1985). On the other hand, turbulent motions tend to sweep the field lines together at convergence points of the flow component perpendicular to them; thus, the field becomes concentrated in flux tubes (Weiss 1964; Proctor & Weiss 1982). This process of *flux concentration* is thought to be aided by the fact that magnetic fields tend to inhibit turbulent motions and, thus, turbulent diffusion.

In homogeneous stationary MHD turbulence, the fine structure of the magnetic field is essentially determined by a dynamical equilibrium of these two main processes. This leads to an intermittent field structure where at any given instant of time most of the magnetic flux is concentrated into thin flux tubes of about equipartition strength that, however, possess a lifetime not exceeding by much the turbulent correlation time. In inhomogeneous and/or nonstationary situations, however, it may often happen that a flux tube gets into an environment where its flux and/or field strength far exceed the values corresponding to the local turbulent equilibrium described above. In such situations, one may expect that turbulent diffusion will dominate over concentration, leading to the slow dissolution of the tube. A case in point are sunspots, which are good examples of such oversized and overintense flux tubes (as compared with the local turbulence scales). They are seen to decay in a few weeks after their formation in a way very much reminiscent of turbulent diffusion (Zwaan 1968). A similar process of dissolution might be expected in the case of the toroidal flux

bundles lying near the bottom of the solar convective zone: they may provide another example of oversized and overintense flux tubes if their sizes and strengths are inferred correctly from flux loop emergence models. A detailed analysis of such a turbulent decay of magnetic flux tubes is, however, complicated by the fact that magnetic fields with energy densities comparable to or exceeding the turbulent kinetic energy density inhibit turbulence and thereby reduce  $\nu$  by a significant amount. The exact form of the relation  $\nu(B)$  is poorly known. (See Kitchatinov, Pipin, & Rüdiger 1994 for a formula valid under certain assumptions.) However, from energy considerations it is clear that in the limit  $B \rightarrow 0$ ,  $\nu(B)$  should tend to the kinematic value  $\nu_0 \sim lv$ , while, in the strong field limit  $B \rightarrow \infty$ , it must go to zero. At the equipartition field value, one may expect a reduction by a factor of order unity.

The strong inhibition of turbulence inside tubes with field strengths well above the equipartition value (as in the case of the two examples mentioned above) suggests that the decay mostly advances by the “gnawing” action of the external turbulent motions on the edges of the tube. This was first proposed by Simon & Leighton (1964), who called this process the *erosion* of the flux tube. They proposed that erosion by supergranular motions was responsible for the decay of sunspots. Smaller scale granular motions may, however, be better suited for this task than the large-scale supergranules.

This paper is an attempt at a detailed study of the turbulent erosion process of magnetic flux tubes outlined above. For simplicity, we consider an axisymmetric magnetic flux tube and disregard the variation of physical quantities along the axis of the tube, assuming that their length scale is large compared with the tube radius. For the nonlinear dependence of the magnetic diffusivity  $\nu$  on the field strength  $B$ , we consider a simple analytic function satisfying the basic physical requirements. We note that the magnetic field in general leads to an anisotropic diffusivity, so that, strictly speaking, our  $\nu$  is just the  $rr$  component of the diffusivity tensor in cylindrical coordinates. With these assump-

tions, we write down and numerically solve the nonlinear diffusion equation governing the problem in § 2. We show that a steep *diffusion front* is easily formed at the boundary of the tube when the internal field strength is large compared with the equipartition value. This front slowly advances into the tube, thus removing magnetic flux from it that is diffused outward into the surrounding weak field region. Section 3 contains an analytical study of the problem, including the calculation of form-invariant propagating solutions (§ 3.1) and estimates of the velocity of the front (§ 3.2) and of its thickness (§ 3.3). In § 4 we will consider some implications of our results for toroidal flux tubes rising in the convection zone and sunspots.

The problem of diffusion with a diffusivity dependent on the variable being transported appears also in other physical and astrophysical contexts such as turbulence propagation or viscous gravity currents (Barenblatt 1983; Gratton & Minotti 1990). An interesting case is heat conduction in a plasma with conductivity,  $\kappa$ , given by Spitzer's formula ( $\kappa \propto T^{5/2}$ ). The strong dependence on  $T$  gives rise in this case to *conduction fronts*, which are relatively abrupt transitions from high to low temperatures. In that case, the front becomes steeper toward low temperatures. In the magnetic case, in contrast, the diffusivity is *suppressed* by the higher fields. Hence, we expect the *magnetic diffusion front* (i.e., the current sheet) to become steeper toward higher field intensities, as in a *mesa-like* mountain profile (see Fig. 1*d* below). An important difference between the thermal and magnetic problems is the possibility of a stationary situation: in the thermal problem, one can compensate for the energy being conducted with adequate amounts of heating and cooling on the hot and cold ends, so that a stationary situation may ensue (as found in different astrophysical contexts). In the problem of a magnetic diffusion front around a flux tube, in contrast, there are no source terms for the magnetic flux inside the tube, so stationarity can only be achieved, if at all, through an external advection term that brings back to the tube the magnetic flux that the ohmic diffusion is trying to remove from it.

## 2. THE NONLINEAR DIFFUSION PROBLEM

### 2.1. Formulation of the Problem

As a first approach to the problem of the nonlinear diffusion of a magnetic field from a magnetic flux tube, we set out to solve a nonlinear one-dimensional diffusion equation with axial symmetry. The one-dimensionality may limit its application to actual solar problems (see § 4), but it has the advantage of retaining the main nonlinear effects while keeping the problem relatively simple. The diffusion equation for the magnetic field in cylindrical coordinates reads

$$\frac{\partial}{\partial t} (rB) = \frac{\partial}{\partial r} \left[ rv(B) \frac{\partial B}{\partial r} \right], \quad (1)$$

where the notations are  $r$  for radius,  $t$  for time,  $B$  for magnetic flux density, and  $v$  for magnetic diffusivity. The inhibiting action of the magnetic field on turbulence is contained in the form of the function  $v(B)$ , which should therefore have the following properties:

a)  $\lim_{B \rightarrow 0} v = v_0$ , where  $v_0$  is the unperturbed value of the diffusivity.

b)  $v/v_0 \in \mathcal{O}(1)$  and  $(1 - v/v_0) \in \mathcal{O}(1)$  if  $B \sim B_e$ , where  $B_e$  is that value of the field intensity for which  $v$  is reduced by 50%. We can expect  $B_e$  to be on the order of the equi-

partition flux density corresponding to a magnetic energy density that equals the kinetic energy density of turbulence.

c)  $v/v_0 \ll 1$  for  $B/B_e \gg 1$  (assuming that the molecular diffusivity is negligible).

A simple function satisfying the above requirements is

$$v(B) = \frac{v_0}{1 + |B/B_e|^{\alpha_v}}. \quad (2)$$

The parameter  $\alpha_v$  determines the steepness of the diffusivity cutoff near  $B_e$ . All the results presented below were computed with the above form of  $v(B)$ ; however, test runs with other forms of  $v(B)$  compatible with conditions *a* through *c* yield qualitatively similar findings. Furthermore, in § 3.3 below we will argue that the general behavior of the solutions should be similar for all forms of  $v(B)$  obeying the criteria listed above.

As the initial condition we again choose simple analytic  $B(r)$  profiles of the form

$$B(r) = \frac{B_0}{1 + (r/r_0)^{\alpha_B}}, \quad (3)$$

with  $\alpha_B = 22$  (to model a tube with constant field strength inside), or

$$B(r) = B_0 \exp\left(-\frac{r^2}{r_0^2}\right) \quad (4)$$

for a tube with a field profile gradually decreasing outward.

### 2.2. Numerical Solutions

Equation (1) is a nonlinear flux-conserving equation that may be solved by standard finite-differencing techniques. A two-step Lax-Wendroff scheme was applied for this purpose. In the numerical calculations, and whenever dimensionless quantities are implied in the paper, the following units were used:  $r_0 = v_0 = B_e = 1$ . (Note that the unit of time is thus the diffusive timescale  $r_0^2/v_0$ .)

For the solution one should also specify the boundary conditions. At  $r = 0$ , the boundary condition is set by the requirement of symmetry, while at the outer boundary we experimented with different forms of the boundary condition to find that if this boundary is sufficiently far away (at  $r = 10$ ) the form of the boundary condition exerts a negligible influence on the results in the physically interesting regime  $r < 2.5$  (in the figures, only this interior regime is shown). Consequently, for all calculations we set the outer boundary at  $r = 10$  as  $\partial B/\partial r = 0$ . The outer fictive points necessary for the Lax-Wendroff method were computed with the neglect of third derivatives; this method preserves the second-order accuracy of the scheme.

The stability criterion  $\Delta t \leq (\Delta x)^2/2v$  seriously limits the time step; therefore, owing to the finite available CPU time, the maximal spatial resolution that could be attained was 8000 grid points (uniformly distributed in the range  $0 \leq r \leq 10$ ), with a corresponding time step of  $10^{-5}$ .

Figure 1 presents the time evolution of the field profiles with the initial condition given by equation (3) with  $\alpha_B = 22$  and for different values of the coefficient  $\alpha_v$  in equation (2), namely, the fully linear case,  $\alpha_v = 0$  (Fig. 1*a*), and the other three cases, which yield increasingly steep profiles (Figs. 1*b*, 1*c*, and 1*d*, with  $\alpha_v = 2, 3, 7$ , respectively). For low  $\alpha_v$  the solution is still similar to the linear constant-diffusivity

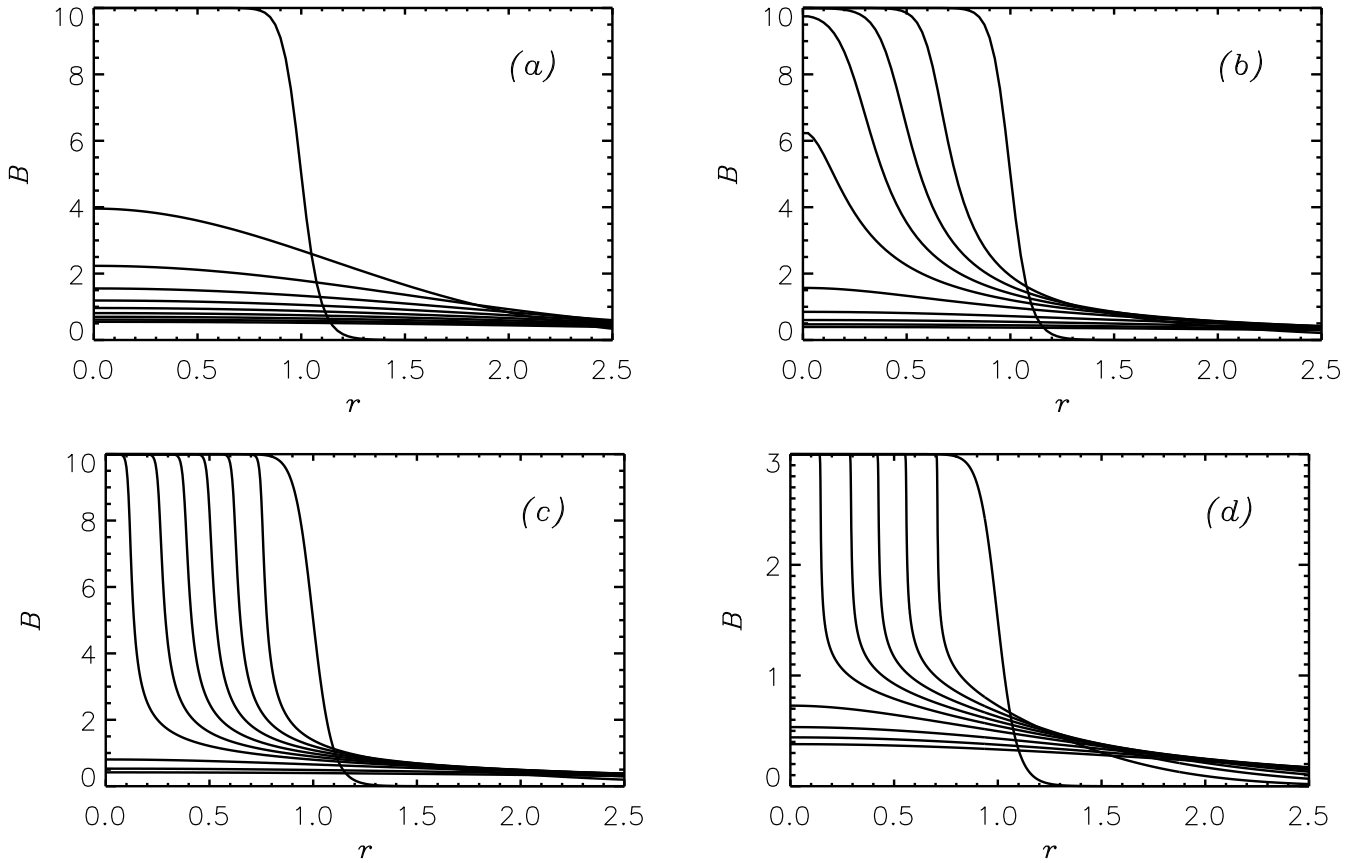


FIG. 1.—Nonlinear turbulent diffusion of a magnetic flux tube. Shown are snapshots of the magnetic field profiles at 10 equally spaced instants of time (with time steps  $\Delta t_0$ , in units of the diffusive timescale) for a magnetic diffusivity of the form of equation (2) with (a) linear limit,  $\alpha_v = 0$ ,  $\Delta t_0 = 0.5$ ; (b)  $\alpha_v = 2$ ,  $\Delta t_0 = 1$ ; (c)  $\alpha_v = 3$ ,  $\Delta t_0 = 1$ ; and (d)  $\alpha_v = 7$ ,  $\Delta t_0 = 0.25$ . Nondimensional units are defined in § 2.2.

case; namely, it is characterized by a monotonic decrease of field gradients, smoothing out the field distribution, and by a gradual decrease of the flux density at  $r = 0$ . However, for higher values of  $\alpha_v$ , a qualitatively new behavior sets in: in a short interval of the radius, the field gradient (or, equivalently, the current density  $j_\phi = -4\pi/c \partial B/\partial r$ ) greatly increases, i.e., a *current sheet* is formed spontaneously. The flux density on the axis remains constant until the arrival of the current sheet, and then it suddenly drops to nearly zero. The sheet moves inward with an essentially constant speed, thereby leading to a nearly parabolic decay law for the flux and area inside it (see Fig. 2). Within about the equipartition radius,  $r \lesssim r_e$ , where  $B(r_e) = B_e$ , the overall form of  $B(r, t)$  is consistent with a dependence of the form  $B(u)$ , where  $u$  is the distance from the current sheet, with no explicit time dependence. In what follows we will call solutions of this type *erosional solutions*, a name that reflects the fact that the formation and inward propagation of the current sheet are due to the eroding action of turbulent magnetic diffusivity on the outskirts of the tube, while in the tube interior diffusion is practically absent.

The thickness of the current sheet quickly decreases with increasing values of  $\alpha_v$ . This limits the possibility of calculating numerically the solutions for high  $\alpha_v$ . The highest value for which we still had good resolution,  $\alpha_v = 7$ , was reached by keeping  $B_0$  at a moderate value of 3 (Fig. 1d). In this case, the current sheet extends just to  $B \sim B_e$ ; from there outward there is a range of radii where the solution quickly approaches the solution of a linear diffusion

problem. For higher values of  $\alpha_v$ , this transition range shrinks to basically just the point where  $B = B_e$ . In that case, a near discontinuity in the derivative of the field profile (i.e., in the current density) appears.

Figures 3 and 4 show the propagation velocity  $w$  of the current sheet as a function of  $\alpha_v$  and  $B_0$ , respectively. The velocity  $w$  was determined by measuring the horizontal separation of consecutive  $B(r)$  curves at different times and  $B$  values inside the current sheet. For a constant internal

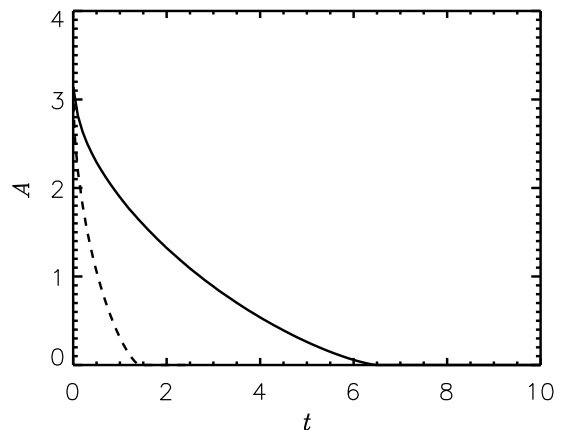


FIG. 2.—The area enclosed within the current sheet as a function of time. The cases  $\alpha_v = 3$  (solid curve) and  $\alpha_v = 7$  (dashed curve) are shown (corresponding to Figs. 1c and 1d).

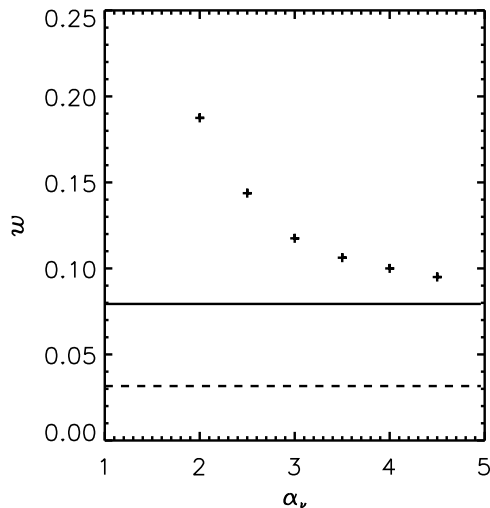


FIG. 3.—Current sheet velocity  $w$  as a function of  $\alpha_v$ , for models with  $B_0 = 10$ ,  $\alpha_B = 22$ , with the limits given by eqs. (16) (solid line) and (15) without the  $3^{-1/2}$  factor (dashed line).

field strength,  $1/w$  is a good estimate of the total lifetime of the tube. While the lifetime increases approximately linearly with  $B_0$ , it seems to saturate to a finite asymptotic value with increasing  $\alpha_v$  when  $B_0$  is constant. This asymptotic value is approximately  $B_0$ .

The magnetic flux that is being removed from the strong-field region is diffused away outward from the current sheet. The rate of removal of flux is roughly  $2\pi r_{CS} w B_0$ , where  $r_{CS}$  is the radius of the current sheet. Given the form invariance of the solutions shown in the panels of Figure 1 with higher  $\alpha_v$ 's, we can expect the flow of magnetic flux across the current sheet to be essentially constant: flux cannot accumulate (nor the contrary) within the sheet if it is to keep a constant shape in time. Hence, the following quantity, the magnetic flux removal rate,  $[wB - v(B)\partial B/\partial r]$  should be constant in the whole strong-field range and across the current sheet. This is borne out by the numerical solutions: Figure 5 shows that the profile of that quantity (long-dashed curve) is basically constant from  $r = 0$  out to the neighborhood of  $B = B_e$ . Thereafter, it smoothly increases: in the

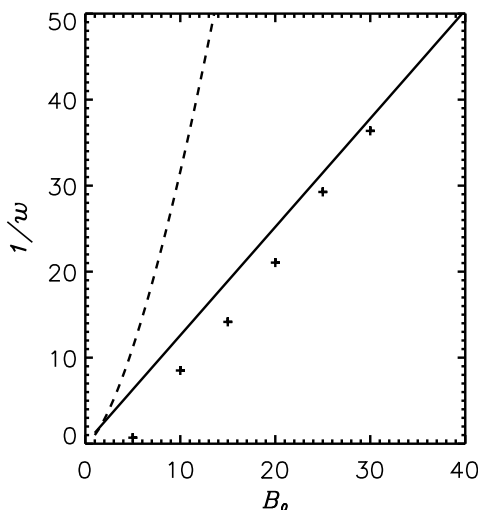


FIG. 4.—Inverse of current sheet velocity  $1/w$  as a function of  $B_0$  for models with  $\alpha_v = 3$ ,  $\alpha_B = 22$ , with the limits given by eqs. (16) (solid line) and (15) without the  $3^{-1/2}$  factor (dashed line).

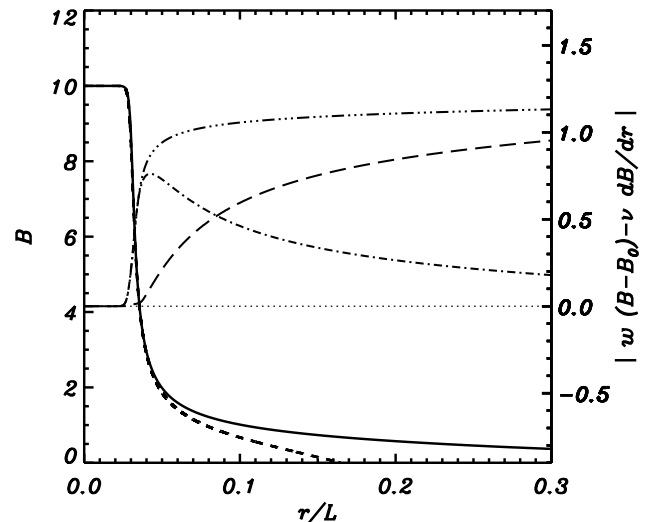


FIG. 5.—Plot of  $w(B - B_0) - v(B)\partial B/\partial r$  (long-dashed curve) for an intermediate time of the solutions of Fig. 1 with  $\alpha_v = 3$ . In the figure, the numerical solution for  $B$  (solid curve) and the corresponding analytical propagating solution (short-dashed curve) are shown with ordinates on the left y-axis. Two further curves are shown with ordinates on the right y-axis:  $-v(B)\partial B/\partial r$  (dash-dotted curve) and  $-w(B - B_0)$  (dash-triple-dotted curve). The constancy of the long-dashed curve to the left of and within the current sheet is a direct consequence of the form-invariance of the erosional solutions.

diffusive part there cannot be a form invariance, since the magnetic flux must increase along time to accommodate what is being removed from inside.

The existence of this class of erosional solutions is not limited to the case of the initial conditions given by equation (3). Figure 6 shows that such solutions are also found with sufficiently high values of  $\alpha_v$  for other initial conditions, the only difference being that for an internal magnetic field depending on  $r$  the propagation velocity of the current sheet is not constant anymore.

Up to this point we tacitly assumed that the value  $v_0$  of the diffusivity outside the tube is constant. This corresponds to a case where the size of turbulent eddies is small compared with the size of the tube. In the alternative case when the turbulent eddies are large, only the small-scale turbulence (with scales below the tube radius) may contribute to the diffusivity, while larger scale motions will simply lead to

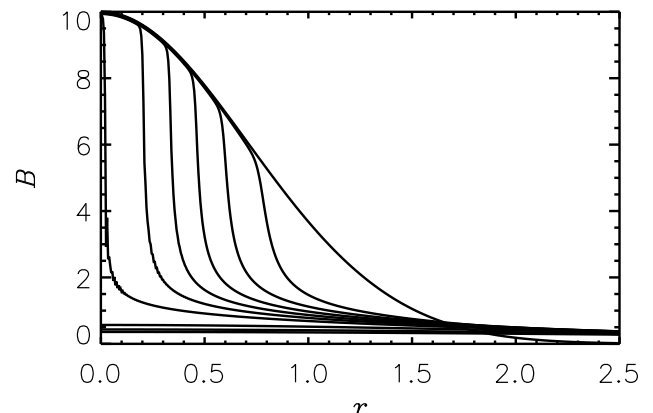


FIG. 6.—Same as Fig. 1, but with a Gaussian profile as initial condition (4),  $\alpha_v = 3.5$ ,  $\Delta t_0 = 1$ . The velocity of erosion is no longer constant but, rather, decreases for increasing field on the strong end of the current sheet.

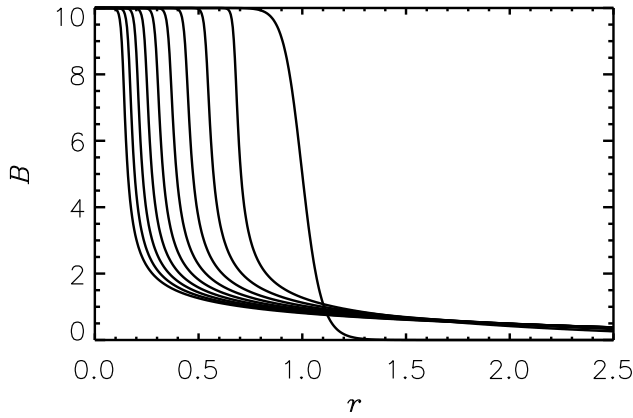


FIG. 7.—Same as Fig. 1c, but using a cutoff for the size of the turbulent elements equal to the tube radius and a Kolmogorov spectrum for the turbulence, with  $\Delta t_0 = 2$ . The value of  $v_0$  in eq. (2) then becomes a function of the tube radius and the decay of the tube is strongly decelerated.

the translational motion of the tube as a whole. Assuming a Kolmogorovian spectrum, the diffusivity scales as  $r_{CS}^{4/3}$ . A solution with such a *rescaling* of  $v_0$  in each time step to the appropriate value of  $r_{CS}$  (assuming  $v_0 = 1$  at  $t = 0$ ) is illustrated in Figure 7. The decay of the tube suffers a strong deceleration with time, making the total lifetime of the tube effectively infinite; however, a significant fraction (e.g., 50% or 90%) of the total flux is still lost on a timescale comparable to that of the solution without rescaling.

3. ANALYTICAL SOLUTIONS AND ESTIMATES

Among the features of the numerical solutions discussed above, some merit particular attention. In the present subsection we clarify and substantiate some of them using analytical considerations. This allows us to extrapolate them to the numerically unattainable limit  $\alpha_v \rightarrow \infty$  as well.

3.1. Propagating Solutions

The numerical results show that in the case of a constant internal flux density, for sufficiently strong nonlinearity (i.e., for sufficiently high values of  $\alpha_v$  and/or  $B_0$ ), the solution in the regime  $B \gtrsim B_e$  approximates a form-invariant *propagating solution* of type  $B = B(r + wt)$ , with  $w$  approximately constant. This invariant shape is reached within a diffusion timescale  $r_0^2/v_0$ .

This prompts the question of the existence of purely propagating, form-invariant solutions of the nonlinear diffusion equation (1). To obtain those, we go to the Cartesian limit of the equation (with spatial coordinate  $x$ ) and try to obtain solutions that depend on  $t$  and  $x$  through the combination  $u \stackrel{\text{def}}{=} x + wt$ , where  $w$  is a constant value (a positive  $w$  means a solution moving toward smaller spatial coordinate, as in the numerical solutions). The corresponding equation is

$$\frac{d}{du} \left[ -wB + v(B) \frac{dB}{du} \right] = 0. \tag{5}$$

This equation has as immediate solution the following class of functions:

$$u - u_c = \int \frac{v(B)}{K + wB} dB, \tag{6}$$

where  $u_c$  and  $K$  are two integration constants. Equation (6) gives  $B$  implicitly as a function of  $u - u_c$ . This class of solu-

tions (eq. [6]) has a flat, exponential asymptote for  $B \rightarrow -K/w$ , which, therefore, may serve to describe the flat region shown by the numerical solutions of the previous section toward  $r \rightarrow 0$ . We then write  $-K/w = B_0$ , introduce the notation  $b = B/B_e$ ,  $B_0 = B_0/B_e$ , and use the form (eq. [2]) for  $v$  so that the solution (eq. [6]) becomes

$$u - u_c = \frac{v_0}{w} \int \frac{db}{(1 + |b|^{\alpha_v})(1 - b/b_0)}. \tag{7}$$

The integral in equation (7) can be easily carried out analytically for integer  $\alpha_v$  (although the solution becomes somewhat unmanageable for  $\alpha_v \gtrsim 5$ ) or, numerically, for arbitrary  $\alpha_v$ . For instance, for  $\alpha_v = 2$  one obtains

$$u - u_c = \frac{v_0}{w} \frac{b_0}{1 + b_0^2} \left[ b_0 \arctan b + \log \frac{(1 + b^2)^{1/2}}{1 - b/b_0} \right]. \tag{8}$$

The form of the solutions (eq. [7]) is illustrated in Figure 8 for four different cases, namely,  $\alpha_v = 2$  (dotted line),  $\alpha_v = 3$  (dot-dashed line),  $\alpha_v = 7$  (dashed line), and a very steep case,  $\alpha_v = 50$  (solid line), which illustrates well the limit  $\alpha_v \rightarrow \infty$ . The increasing nonlinearity makes the transition between the diffusive and nondiffusive regions increasingly steep, similarly to the case of heat conduction with nonlinear conductivity coefficient. For  $\alpha_v = 50$ , in particular, the current sheet is very narrow, with a sharp transition to the asymptotic horizontal regime. For  $B \lesssim B_e$ , the four solutions are qualitatively similar and approach a linear diffusive solution. In these plane-parallel solutions, there is no natural length scale imposed by the equations: solutions exist for arbitrary  $w > 0$  values, independent of  $B_0$ . A change in  $w$  does not change the shape of the solution, but only its length scale, which is  $v_0/w$ . In contrast, in the actual axisymmetric problem, a length scale is set by the radius  $r_0$  of the initial tube, and  $w$  can no longer be specified arbitrarily (see § 3.2 below).

We expect the propagating solutions to fit increasingly well the numerical solutions of the previous section the higher the value of  $\alpha_v$  and  $b_0$  and, at any rate, for  $b \gtrsim 1$ . The goodness of the fit can be seen in Figure 9, which contains the numerical (dotted line) and analytical (dashed line) solu-

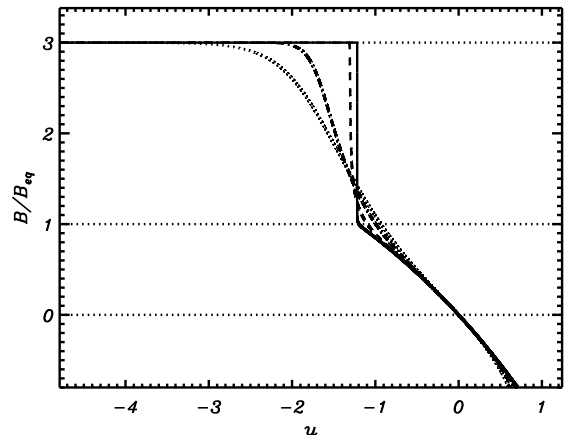


FIG. 8.—Analytic solutions for a plane-parallel form-invariant propagating solution of the nonlinear diffusion eq. (6) with  $B_0 = 3$  and  $\alpha_v = 2$  (dotted line),  $\alpha_v = 3$  (dot-dashed line),  $\alpha_v = 7$  (dashed line), and  $\alpha_v = 50$  (solid line).  $u$  is dimensionless in this figure, the unit is  $v_0/w$ . The near discontinuity of the current density at the lower end of the current sheet is clearly discernible in the steepest case.

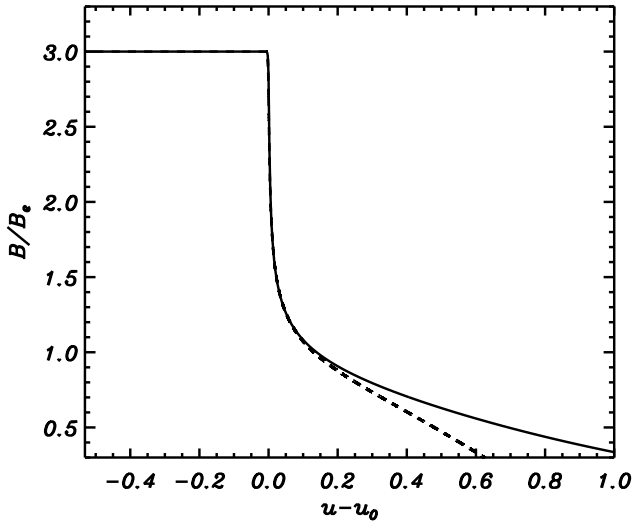


FIG. 9.—Comparison of the analytical (dashed line) and numerical (solid line) solutions for  $B_0 = 3$  and  $\alpha_v = 7$ . The analytical solution was computed with the  $w$  value determined from the numerical solution, and the arbitrary horizontal offset was set to optimize the agreement.

tions for the case  $\alpha_v = 7$  with  $B_0 = 3$ . The fit is excellent in the whole nonlinear region.

The propagating solutions cannot approximate the numerical solution well outside the current sheet for fundamental reasons: the current sheet is a region where magnetic flux is being taken away from the tube and transported outward. To have a fully form-invariant solution, there should be a mechanism to exactly dispose of this flux in the outer regions of the domain. The latter can be, for example, a flux-shedding boundary condition or some internal device that causes the loss of magnetic flux (which should play a role like the cooling in a thermal problem). We have none of these, and, as a consequence, (a) the numerical solution is not form-invariant in the weak-field range, and (b) the analytical solution goes to negative field values at some distance of the flux tube (see Fig. 8).

The establishment of a form-invariant propagating region along the time evolution of the system may then be qualitatively understood as follows. The high diffusivity in the outskirts ( $B \lesssim B_e$ ) of the tube removes the flux in that domain in about one diffusive timescale  $r_0^2/\nu_0$ , while the strong internal field at  $r < r_{CS}$  effectively inhibits any significant flux loss from the internal region over such short time-scales. As a consequence, a steep field gradient (i.e., a current sheet) forms. The gradient increases until the smoothing effect resulting from the diffusive flux loss can balance the nonlinear steepening. This is exactly the balance responsible for the form-invariant nature of the exact analytic solution of equation (5), which is therefore a good approximation of the solution in the regime  $B \gtrsim B_e$ . This property of the erosional solution may be utilized in deriving a formula for the thickness of the current sheet (see § 3.3 below).

### 3.2. Current Sheet Velocity

From the numerical solutions, the velocity  $w$  of the inward propagation of the solution (and of the current sheet in particular) appears to increase linearly with  $B_0$  and to become asymptotically independent of  $\alpha_v$  for high  $\alpha_v$  values, i.e., for increasingly effective magnetic inhibition of turbu-

lence. This implies that the lifetime of flux tubes remains finite even in the limit of  $\alpha_v \rightarrow \infty$ , i.e., for infinitely effective inhibition of turbulence inside the tube! Although Figure 3 strongly suggests such a behavior, a strict proof of this result clearly cannot be given on the basis of numerical results alone. Below we demonstrate with approximate analytical methods that a lower limit for  $w$  indeed exists. Here we concentrate on the case of a flux tube with constant internal flux density and a corresponding form-invariant propagating  $B(u)$  profile in the erosional solution. It is, however, clear that for tubes with the same value of  $B_0$  but outward decreasing field strength the efficiency of the erosion process can only increase.

The analytical results for the plane-parallel case (see § 3.1 above) are of no help in the present problem since these solutions exist for any value of  $w$ . It is clear from a dimensional analysis that the most generic combination of the parameters entering the problem ( $\nu_0, \alpha_v, r_0, B_e, B_0$ ) with velocity dimensions is  $f(B_0/B_e, \alpha_v)\nu_0/r_0$ . Our task consists of determining the form of the function  $f(B_0/B_e, \alpha_v)$  in the limit  $\alpha_v \rightarrow \infty$ .

To obtain that function, note that in that limit the current sheet becomes infinitely narrow, is placed precisely at the equipartition radius,  $r = r_e$ , and coincides in its full extent with the current sheet of the corresponding form-invariant propagating solution. Moreover, the transition between the current sheet and the  $v = v_0$  regime occurs sharply at  $B = B_e$ . In fact,  $v(B)$  will have a near discontinuity at  $B = B_e$  and so will the derivative  $\partial B/\partial r$ . We saw in the previous section that the form invariance implied that the flow of magnetic flux,  $wB - v(B)(dB/dr)$ , was constant in the whole form-invariant section of the solution down to the lower end of the current sheet (and slowly departs from the constant value when going outward from it). In our case, this means that that quantity is constant down to  $B = B_e$ . Using all these facts, we can now obtain a first estimate for the velocity of the current sheet. Equating the values of that quantity on both ends of the current sheet, we obtain

$$wB_0 = wB_e - v_0 \left( \frac{\partial B}{\partial r} \right)_{B=B_e}, \quad (9)$$

where the last derivative is meant as the limit value when one approaches  $B = B_e$  from *outside* the current sheet. This leads to

$$w = \frac{v_0}{r_1} \frac{B_e}{B_0 - B_e}, \quad (10)$$

with

$$\frac{1}{r_1} \stackrel{\text{def}}{=} - \frac{1}{B_e} \left( \frac{\partial B}{\partial r} \right)_{B=B_e}. \quad (11)$$

The question is now how to determine  $r_1$  in equation (10). An upper limit can be set by noting that outside the current sheet, i.e., for  $r > r_e$ ,  $\partial^2 B(r)/\partial r^2 > 0$ , so that the straight line  $B = B_e[1 - (r - r_e)/r_1]$ , tangential to the solution at  $r_e$ , certainly runs below the actual field distribution. The latter, then, contains more magnetic flux than the straight line. Using the approximation  $\Phi_0 \approx \pi r_0^2 B_0$ , where  $\Phi_0$  is the total magnetic flux in the whole domain, we have

$$2\pi B_e \int_{r_e}^{r_e+r_1} \left[ \frac{1 - (r - r_e)}{r_1} \right] r dr < \pi B_0 (r_0^2 - r_e^2). \quad (12)$$

This inequality should be valid at any stage after the moment when the form-invariant propagating solution finally sets in and  $r_1$  settles to a basically constant value. In order to determine the constraint on  $r_1$ , it suffices to know the value of  $r_e$  at that instant. A lower limit for this value is obviously zero, so solving the inequality (12) for  $r_1$ , we get

$$r_1 < -\frac{3}{2}r_e + \left[ \frac{9}{4}r_e^2 + 3\frac{B_0}{B_e}(r_0^2 - r_e^2) \right]^{1/2} < \left( \frac{9}{4}r_e^2 + 3\frac{B_0}{B_e}r_0^2 \right)^{1/2}. \quad (13)$$

Now, in the high- $\alpha_v$  limit, the current sheet is very thin, so that  $r_e < r_0$ . This yields

$$\frac{r_1}{r_0} < \left( \frac{9}{4} + 3\frac{B_0}{B_e} \right)^{1/2}. \quad (14)$$

Using equation (10) we obtain the following lower bound for  $w$  in the limit  $B_0 \gg B_e$ :

$$w > \frac{v_0}{r_0} \frac{1}{\sqrt{3}} \left( \frac{B_e}{B_0} \right)^{3/2}. \quad (15)$$

We note without going into similar details that replacing the above straight line with a logarithmic profile [stationary solution of the linear diffusivity equation with the boundary condition  $B(r_e) = B_e$ ] would lead to a transcendental equation instead of the second-order equation (12). Its solution yields a condition nearly identical to inequality (15) without the factor  $3^{1/2}$ . How good this lower bound for  $w$  is can be seen in Figures 3 and 4, where the dashed line represents the right-hand side of equation (15) (or its inverse, in the case of Fig. 4), without the  $3^{1/2}$  factor.

A more realistic estimate of the value of  $r_e$  at the time when the erosional solution sets in can be given taking into account that the initial transient phase physically consists of the period when the diffusive *gnawing* of the outer parts of the tube increases the gradient further in. Thus, one may expect the duration of the transient phase to be  $t_{tr} \sim r_0^2/v_0$ , i.e., the diffusion timescale. With this, one has approximately  $r_e(t = t_{tr}) \sim r_0(1 - wr_0/v_0)$ . Inserting this condition into the inequality (15) (or, better still, into the equivalent inequality for the logarithmic profile discussed in the previous paragraph), one obtains a relation between  $w$  and  $r_1$ . This relation, coupled with equation (10), can be solved to find that in the limit  $B_0 \gg B_e$ ,

$$w \gtrsim 2^{-1/3} \frac{B_e}{B_0} \frac{v_0}{r_0}. \quad (16)$$

This new lower bound (represented as a solid line in Figs. 3 and 4) turns out to give a very good approximation to the numerical results for  $w$ . In fact, the value of the coefficient  $2^{-1/3}$  in equation (16) shows only weak sensitivity to arbitrary order-of-unity factors in the expression of  $t_{tr}$  and in the upper limit used in the integral constraint (typical changes are by  $\pm 0.1$ ). Equations (16) and (10) then clearly also imply that  $r_1$  and  $r_0$  are of the same order of magnitude.

Closing this subsection, we should stress that the validity of the results derived here is not confined to the particular choice of the  $v(B)$  function given in equation (2), as this particular form was used nowhere. For more general profiles, the parameter  $\alpha_v$  may simply be defined so that the

relation

$$\frac{B_e}{v_0} \left( \frac{dv}{dB} \right)_{B_e} = -\frac{\alpha_v}{4} \quad (17)$$

remains valid, i.e.,  $\alpha_v$  simply parameterizes the steepness of the diffusivity cutoff at  $B_e$ . It is easy to see that all the above results remain valid in this more general case.

### 3.3. Current Sheet Thickness

Both in the numerical results of § 2.2 and in the propagating solutions of § 3.1 the thickness of the current sheet rapidly decreases for increasing  $\alpha_v$ . In this section we obtain an analytical estimate for this dependence and show that, in fact, the current sheet thickness has a power-law dependence on the internal field strength,  $B_0/B_e$ , with exponent  $-\alpha_v$ . We show this for the analytical solutions of § 3.1. The result is then immediately applicable to the numerical erosional solutions with high  $\alpha_v$ , given the excellent agreement between them.

In the current sheet, the field distribution must go through an inflection point. Define the thickness of the current sheet as the scale length of  $B(r)$  at that point. Using equation (5), we get

$$\Delta \equiv -B_i \left( \frac{dB}{du} \right)_i^{-1} = -\frac{B_i}{w} \left( \frac{dv}{dB} \right)_i = \frac{v_i^2}{v_0} \frac{\alpha_v}{w} \left( \frac{B_i}{B_e} \right)^{\alpha_v}, \quad (18)$$

where the index  $i$  refers to values at the inflection point. Substituting here inequality (16),

$$\frac{\Delta}{r_0} \lesssim 2^{1/3} \alpha_v \left( \frac{v_i}{v_0} \right)^2 \frac{B_0}{B_e} \left( \frac{B_i}{B_e} \right)^{\alpha_v}. \quad (19)$$

Next we show that in the high- $\alpha_v$  limit the inflection point occurs high up in the current sheet, i.e.,  $B_i \rightarrow B_0$ . At the inflection point one, has  $d^2u/dB^2 = 0$ ; using the general integral (eq. [6]) of the plane-parallel form-invariant propagating solution, this implies

$$\frac{1}{v_i} \frac{dv_i}{dB} = \frac{1}{B_i - B_0}. \quad (20)$$

Substituting here the expression (2) of  $v(B)$ , we find

$$\alpha_v \left( \frac{B_0}{B_i} - 1 \right) = 1 + \left( \frac{B_i}{B_e} \right)^{-\alpha_v}, \quad (21)$$

the high- $\alpha_v$  limit of which is indeed

$$B_i \rightarrow \frac{B_0}{1 + 1/\alpha_v} \rightarrow B_0. \quad (22)$$

Comparing this with equation (19), and using the limit  $B_0 \gg B_e$ , we finally obtain

$$\frac{\Delta}{r_0} \lesssim 2^{1/3} \alpha_v \left( \frac{B_0}{B_e} \right)^{1-\alpha_v}, \quad (23)$$

which was to be shown.

## 4. APPLICATIONS

The solar magnetic field appears in the form of magnetic flux tubes of different sizes in the solar atmosphere. Through the studies of the emergence of the active region fields, as well as from general theoretical results of magnetoconvection and MHD turbulence, one assumes that also the magnetic field in the convection zone may be in the form of

individual flux tubes or bunches of them. For the application of the one-dimensional results of the foregoing sections to the Sun, the magnetic flux tubes must be, even if only approximately, cylindrically symmetric. In our case, a necessary condition for this is that the length scale of variation of properties along the tube axis be much larger than transversely to it (e.g., the tube radius must be much smaller than all local stratification scale heights). Under this condition (typical, for instance, of the so-called thin-flux-tube [tft] approximation), equation (1) can be used to describe approximately the diffusion of field through the surrounding turbulence. We stress that while the assumption of cylindrical symmetry is a common feature of our models and of the tft formalism, yet here we break away from the tft approximation by explicitly considering the field variation across the tube. In the following we consider two cases of current interest, first, one in which the cylindrical shape of the tube is a good approximation, namely, the magnetic tubes in the deep convection zone, and, second, the diffusion of the field in sunspots. Sunspots can be simplified using axisymmetric models; yet, they do not possess cylindrical symmetry, so this case can only be seen as a simple approximation to a far more complex problem.

#### 4.1. Toroidal Flux Tubes at the Bottom of the Solar Convective Zone

It is generally accepted that most of the magnetic flux responsible for solar activity phenomena in general, and for the appearance of active regions in particular, is stored close to the bottom of the solar convective zone (Spiegel & Weiss 1980; see also Moreno-Insertis, Schüssler, & Ferriz-Mas 1992). The question arises whether these toroidal flux bundles are affected by the phenomenon of turbulent erosion modeled above to any significant degree. Using equation (16), the flux loss rate from a tube is

$$-\dot{\Phi} = 2\pi r_{\text{CS}} B_0 w = \frac{2^{2/3} \pi v_0 B_e r_{\text{CS}}}{r_0} = 2^{2/3} \pi v_0 B_e \left( \frac{\Phi}{\Phi_0} \right)^{1/2}, \quad (24)$$

where we used the approximation  $r_{\text{CS}} \simeq (\Phi/\pi B_0)^{1/2}$ , and we took into account that  $r_{\text{CS}}$  and  $\Phi$  are functions of time, while  $w$  is determined by the *initial* radius  $r_0$  (or, equivalently,  $\Phi_0$ ) in the case when the tube is not moving compared with its surroundings. In a situation where a tube is moving through the surrounding plasma (as in the case of *emerging* flux loops) with a significant speed ( $V > v_0/r_0$ ), the external flow relative to the tube will sweep away the weak outer field thereby continuously “reinitializing” the decay; in that case, the *actual*, time-dependent value of  $r_{\text{CS}}$  should be used in the expression for  $w$ , and consequently equation (24) must be replaced by

$$-\dot{\Phi} = 2^{2/3} \pi v_0 B_e \quad (\text{moving tube}). \quad (25)$$

Consider first the implications of equation (24) for magnetic tubes in the deep convection zone. The full turbulent diffusivity there is of order  $v_{00} \sim WH \sim 1000 \text{ km}^2 \text{ s}^{-1}$ , ( $W \simeq 60 \text{ m s}^{-1}$  is the r.m.s. vertical velocity of turbulence), but as the scale of the turbulent eddies is the pressure scale height  $H \sim 5 \times 10^4 \text{ km}$ , i.e., much larger than the tube size, the diffusivity should be rescaled as

$$v_0 = v_{00} \left( \frac{r_0}{H} \right)^{4/3} \sim W \left( \frac{\Phi}{\pi B_0} \right)^{2/3} H^{-1/3}. \quad (26)$$

Writing this into equation (24), we find

$$\dot{\Phi} = -WB_e \left( \frac{4\pi\Phi^2}{HB_0^2} \right)^{1/3} \left( \frac{\Phi}{\Phi_0} \right)^{1/2}. \quad (27)$$

Numerical simulations of the emergence of buoyant magnetic flux loops through the solar convective zone (Moreno-Insertis 1986; D’Silva & Choudhuri 1993; Caligari, Moreno-Insertis, & Schüssler 1995; Fan, Fisher, & McClymont 1994) show that in order to get a satisfactory agreement with the observations of solar active regions, the toroidal flux tubes on which the perturbations develop must have magnetic flux densities of  $B_0 \sim 10^5 \text{ G}$ , while the equipartition field at the bottom of the convective zone is  $B_e \sim 10^4 \text{ G}$ . Those models do not take into account any diffusivity, so, to match the observed fluxes in active regions, the tubes must have magnetic fluxes of order  $10^{22} \text{ Mx}$  also in the deep convection zone. With these values, using equation (27) we find that  $-\Phi/\dot{\Phi} \sim 1$  month for the flux loss timescale. This is very much shorter than the length of the solar activity cycle. While the timescale increases with time owing to the factor  $(\Phi/\Phi_0)^{1/2}$  in equation (27), the greater part of the original flux will still be lost on essentially the initial timescale.

On the basis of such short lifetimes, it appears that flux tubes with the above properties cannot be stored in the lower part of the convective zone for times comparable to the solar cycle. We note however that  $\dot{\Phi}$ , and consequently the timescale, depend rather sensitively (as  $W^2$ , since  $B_e \propto W$ ) on the r.m.s. turbulent velocity. Thus, reducing  $W$  by a factor of 5–10 could increase the decay timescale to several years, comparable to the solar cycle. However, a careful consideration of the possible sources of error, taking into account the results of the relevant numerical simulations (Chan & Sofia 1989; Lydon, Fox, & Sofia 1992; Kim et al. 1996) shows that the  $W$  values derived here are subject to uncertainties not exceeding  $\pm 30\%$ – $40\%$ . In particular, there seems to be no obvious way to reduce  $W$  by more than about 20% at the base of the convective zone. So the flux storage problems mentioned above appear to be unavoidable.

Thus, the calibration of local convection theories to numerical experiments leaves now little room to change  $W$  in the unstably stratified part of the convective zone. On the other hand, our present ignorance regarding the detailed structure of the overshooting layer below still allows the possibility of storing the toroidal flux there.

Turning now to expression (25), we consider the loss of flux in unstable magnetic tubes that rise across the convection zone to produce active regions. To that end, we substitute for  $v_0$  using equation (26) to get

$$\dot{\Phi} = -WB_e \left( \frac{4\pi\Phi^2}{HB_0^2} \right)^{1/3}. \quad (28)$$

A first impression for the orders of magnitude predicted by this formula can be obtained by substituting in it a few time profiles  $z(t)$  and  $B_0(t)$  typical of the tft numerical simulations of the rise of magnetic tubes mentioned above, with  $z$  the depth below the photosphere. Taking, for instance, for  $z(t)$  and  $B_0(t)$  the position and field strength of the summit of the rising loop in the simulations of Caligari et al. (1995), one can obtain  $\dot{\Phi}$  from equation (28). To avoid the added complication associated with the sliding motion of the tube’s mass elements along the field lines, we use here time

profiles corresponding to a nonrotating case ( $\Omega = 0$ ), for which the mass element at the tube summit is fixed along time. On the other hand, one has to substitute for  $W$ ,  $H$ , and  $B_e$  using a stratification model and the following formula:

$$W^3 = \frac{1}{1.37} \nabla_{\text{ad}} \frac{L_{\odot}}{4\pi R^2 \rho} \quad (29)$$

(Kim et al. 1996), where  $\nabla_{\text{ad}}$  was simply taken to be 0.4 (a good approximation except near the surface) and

$$B_e = 4\pi\rho\chi W^2, \quad (30)$$

with the numerical factor  $\chi = 1 + 2.06^2$  taken from Chan & Sofia (1989).

Figure 10 shows the decrease of the magnetic flux during the passage through the convective zone predicted by equation (28) for tubes of different sizes and field strengths. We first use the  $z(t)$  profiles obtained from the thin-flux-tube numerical simulation of the rise of tubes with  $10^{22}$  Mx and  $B_{00} = 1.2 \times 10^5$  G (*solid curve*) or  $B_{00} = 2 \times 10^5$  G (*dash-dotted curve*). We integrate equation (28) downward starting from the surface with that value of flux. We see that these tubes must lose a substantial fraction of their original magnetic flux along the rise (in contrast to the simplifying assumption systematically made in the thin flux tube simulations). The difference between the two curves is due to the shorter timescale of the tube with higher initial field strength. Anyway, both curves show flux values of order  $10^{23}$  Mx in deep levels. So, we repeat the calculation, this time taking  $z(t)$  from a tft simulation with  $10^{23}$  Mx and  $B_{00} = 1.2 \times 10^5$  G (*dashed line*) (but start the integration of eq. [28] at the surface with the same  $\Phi$  value as for the other curves, for easiness of comparison). Here too the tube suffers a substantial magnetic flux loss. However, the calculation shows only a relatively small sensitivity to the initial value of the magnetic flux in the emergence computation. This is because the magnetic flux of the tube enters the tft calculation only via the drag force opposed by the surrounding medium to the advance of the tube. In the range

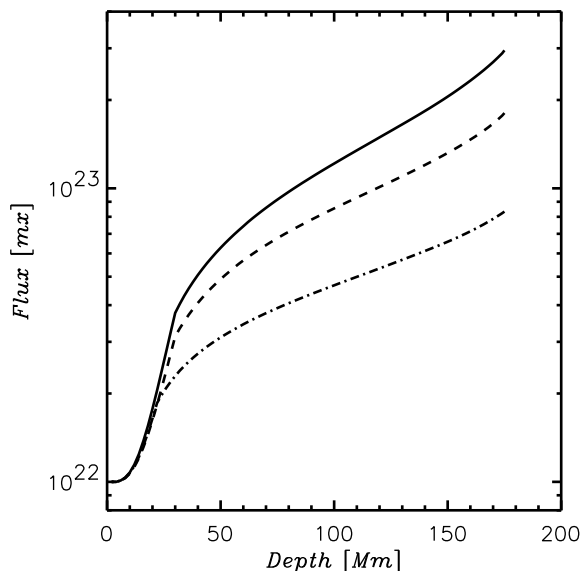


FIG. 10.—Flux loss from flux loops rising through the solar convective zone. *Solid line*:  $\Phi = 10^{22}$  Mx,  $B_{00} = 1.2 \times 10^5$  G. *Dashed line*:  $\Phi = 10^{23}$  Mx,  $B_{00} = 1.2 \times 10^5$  G. *Dash-dotted line*:  $\Phi = 10^{22}$  Mx,  $B_{00} = 2 \times 10^5$  G.

of fluxes of the figure, the radius of the cross section is large enough for the drag force not to play a primary role in determining the speed of rise—hence, the time evolution profile of all quantities in the tube is fairly independent of its magnetic flux. This is a fortunate circumstance as it justifies a posteriori our (strictly speaking, inconsistent) approach of studying flux loss using models computed with the assumption of a constant flux. It is perhaps also adequate to mention at this point that the use of  $z(t)$  and  $B_0(t)$  profiles taken from numerical simulations for a rotating case ( $\Omega = \Omega_{\odot}$ ) yields results basically coinciding with those shown in Figure 10 within a factor 2 at most (yet, the interpretation of the results for the rotating case has to be done with some care, as indicated above).

From all this we conclude that the toroidal flux tubes whose emergence leads to the formation of solar active regions must lose a significant part of their flux by turbulent erosion during their passage through the convective zone. In fact, it would be interesting to include the formulae developed in this section into a tft model, so that one could calculate the time evolution of the magnetic flux in a more self-consistent way. Doing that could result in a nonconstancy of the magnetic flux of the tube as one moves along its axis at any given instant of time. This would be no violation of the solenoidality of the  $B$  field but, rather, would just reflect the fact that the external sheets of a stretch of the tube may at some level detach from its concentrated core and go into a weak-field phase that is no longer counted as part of the tube in the tft model.

#### 4.2. Sunspots

The sharpness of the outer penumbral boundary of sunspots (i.e., the sudden change from filamentary penumbral fine structure to nearly normal granulation in less than a resolution element; Zwaan 1968; Gokhale & Zwaan 1972) is a well-known observational fact that implies the presence of a current sheet around the spot in the photospheric layers. Studies of sunspot structure (Jahn 1989) indicate that a significant part of the currents is also concentrated into a current sheet in larger depths below the surface. The calculations presented above demonstrate how turbulent erosion of the surface of a magnetic flux tube can lead to the spontaneous formation of a current sheet around the tube. We thus propose that the sharp boundary of sunspots may be a natural consequence of turbulent erosion. As observations indicate that pores and sunspots tend to have well-defined boundaries from the beginning of their existence, this process of current sheet formation should occur below the surface, before the eruption of the tube.

With the model developed in this paper, we can attempt to understand some aspects of sunspot decay. That this process may be due to the eroding action of external motions was in fact already proposed by Simon & Leighton (1964). However, one must keep in mind that sunspots are very far from being slender flux tubes, so the application of the present models may only be suggestive, and the resulting formulae very approximative.

The constancy of  $w$  implies a constant flux loss rate/tube surface area; therefore, if one introduces an artificial sink term in the diffusion equation outside the current sheet, thereby increasing the gradient and the flux loss, the decay rate should increase. This was indeed found in a numerical solution. A physical mechanism capable of such flux removal from the neighborhood of a flux tube could be a

transverse flow sweeping away the diffuse field (as with toroidal flux emerging through the convective zone). Again, such processes could only increase the effectiveness of turbulent erosion, thus the lifetime estimates given in these applications should be regarded as rather conservative upper estimates. On the other hand, such a removal of the outer diffuse flux may be regarded as a “renovation” of the initial state, so that the end of the period of effective renovation (i.e., the full emergence of the loop with verticalization of the legs) may be regarded as the instant of time corresponding to  $t = 0$  in our calculations. This may be approximately also the time when the spot area attains its maximal value, so “ $r_0$ ” may represent the maximal radius of the spot.

Using equation (16) the lifetime of a spot in the limit of strong inhibition of turbulence is

$$\frac{r_0}{w} = 2^{1/3} \frac{r_0^2}{v_0} \frac{B_0}{B_e}. \quad (31)$$

Substituting here  $B_0 \sim 3000$  G,  $B_e \sim 400$  G,  $v_0 \sim 1000$  km<sup>2</sup> s<sup>-1</sup> (the granular value), one finds

$$\frac{r_0}{w} = \left( \frac{r_0}{10^4 \text{ km}} \right)^2 \times 10 \text{ [days]}. \quad (32)$$

From this formula it is apparent that the total lifetime is proportional to the initial area of the spot, thus returning the well-known linear area-lifetime relation (Gnevishev 1938). The orders of magnitude are also consistent with observations: in particular, the total lifetime of large, recurrent spots of  $\sim 5 \times 10^4$  km diameter is found to be about 2–3 months.

The area–time decay curves resulting from a current sheet moving inward with a constant velocity are necessarily parabolic, as can be seen in Figure 2 as well. This would run counter the common view that the sunspot decay proceeds linearly in time. There have been suggestions of the parabolic nature of the sunspot decay laws on the basis of a statistical study of large data samples (Moreno-Insertis & Vázquez 1988). The scatter intrinsic to this kind of data, however, makes it difficult to distinguish a parabola with the curvature predicted above from a linear decay law (Martínez Pillet, Moreno-Insertis, & Vázquez 1993). Nevertheless, in a recent analysis, Petrovay & van Driel-Gesztelyi (1997) found decisive observational evidence in favor of a parabolic decay law.

We note that in a parallel work Rüdiger & Kitchatinov (1996) solved the *two-dimensional* nonlinear diffusion equation. As far as it can be judged from their figures, their solution falls in the diffusive regime, with a nearly linear decay law (in apparent contradiction to the observations; cf. Petrovay & van Driel-Gesztelyi 1997). As, however, results from only a single run with one particular choice of initial conditions are available, and the uppermost 1500 km of the convective zone (where  $B/B_e$  would be highest) is not included in the model volume, it is presently not possible to judge the general validity of those findings.

An interesting property of the erosion models is that the *remaining lifetime* of a sunspot with instantaneous radius  $r_{CS}$ ,

$$\frac{r_{CS}}{w} = \left( \frac{r_{CS}}{r_0} \right) \left( \frac{r_0}{10^4 \text{ km}} \right)^2 \times 12 \text{ [days]}, \quad (33)$$

or, equivalently, the area decay rate,

$$2\pi r_{CS} w = \frac{r_{CS}}{r_0} \pi \frac{(10^4 \text{ km})^2}{6 \text{ [days]}}, \quad (34)$$

does not depend only on  $r_{CS}$  but also on  $r_0$ , i.e., on the *initial* radius of the spot.

This is caused by the fact that the value of  $w$  is fixed at an early stage of the decay, when the propagating solution is first adopted, and it does not change much thereafter. This implies that of two observed decaying sunspots with identical radii, the younger one (i.e., the one with a smaller maximal radius) should show a faster decay rate. One may speculate that this dependence on the original size may possibly be a contributing factor to the large intrinsic scatter in the decay rates of sunspots of a given size.

From observations it is known that sunspots are surrounded by a radial outflow, called the moat. It is then interesting to investigate the effects of such an outflow on the solutions. The actual structure of the moat flow is not totally clear: since the field lines are inclined, the flow velocity could have a nonnegligible component parallel to the field lines. However, only the component normal to the field may have a direct effect on its decay. We then use a more general form of the diffusion equation including an advection term due to the radial outflow of matter, and, within the one-dimensionality of the model, disregard any effects due to any other component of the flow. The resulting equation is

$$\frac{\partial}{\partial t} (rB) = \frac{\partial}{\partial r} \left[ rv(B) \frac{\partial B}{\partial r} + v_r rB \right], \quad (35)$$

which substitutes for equation (1). Observations suggest that outside the penumbra the outflow has a velocity of  $\sim 0.5$ – $1$  km s<sup>-1</sup>, nearly independently of the radius (Pardon, Worden, & Schneeberger 1979; Brickhouse & LaBonte 1988). On the other hand, the radial flow must have a sharp cutoff at the boundary of the strong field region. The function  $v_r$  may then be represented as

$$v_r = \frac{2v_0}{1 + (B/B_e)^{\alpha_v}}, \quad (36)$$

where  $v_0$  is the outflow velocity at  $r_e$ . Equation (16) can be readily generalized to yield

$$w \gtrsim 2^{-1/3} \frac{B_e}{B_0} \left( \frac{v_0}{r_0} + v_0 \right). \quad (37)$$

We have obtained numerical solutions for this problem: the resulting field profile can be seen in Figure 11, which presents the case for  $v_0 = 1$ ,  $\alpha_v = 5$ ,  $\alpha_v = 3$ . These solutions confirm the accuracy of the estimate (eq. [37]). Now, the dimensionless value of  $v_0$  will be  $0.5 \text{ km s}^{-1} \times r_0/v_0$ , i.e., crudely in the range  $2 < v_0 r_0/v_0 < 15$ . Consequently, a moat flow perpendicular to the field lines would imply an order-of-magnitude increase in the decay rate, in conflict with the observations. This leads us to conclude that, to the extent that the present models can teach us something about the process of sunspot decay, the moat flow should be mostly parallel to the field lines. This conclusion also agrees with the observations of Skumanich, Lites, & Martínez Pillet (1994) that the *apparent* flux transport rate of the moat (in the form of moving magnetic features, MMFs) greatly exceeds the actual flux loss from the spot.

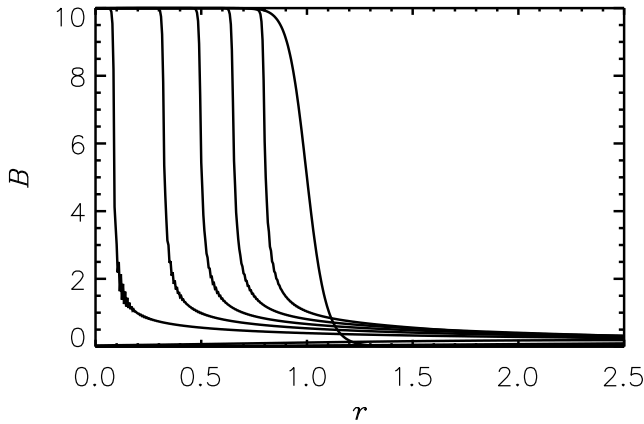


FIG. 11.—Same as Fig. 1c, but including a radial outflow as in eq. (36), with  $v_0 = 1$ ,  $\alpha_v = 5$ ,  $\Delta t_0 = 0.5$ .

## 5. CONCLUSION

An investigation by numerical and analytical means of the solution of the nonlinear axisymmetric diffusion equation (1) with  $v(B)$  functions that satisfy the minimum set of physical requirements listed in § 2.1 yielded the following main results. For sufficiently strong nonlinearity (i.e., for sufficiently strong reduction of  $v$  inside the tube) a current sheet is spontaneously formed around the tube within one diffusion timescale  $r_0^2/v_0$  ( $r_0$  is the initial radius of the tube, and  $v_0$  is the kinematical value of the diffusivity). The field profile in and inside the current sheet is well approximated by the analytical form-invariant propagating solution of the plane-parallel equivalent of equation (1). This sheet propagates inward with a velocity

$$w \sim 2^{-1/3} \frac{B_e v_0}{B_0 r_0}, \quad (38)$$

where  $B_0$  is the field strength just inside the current sheet,  $B_e$  is the equipartition field strength. Accordingly, the lifetime of a tube with constant internal flux density is increased by a factor  $B_0/B_e$ , independent of the value of the diffusivity inside the tube.

On the basis of these results we performed approximate calculations of the magnetic flux loss from toroidal flux

tubes lying at the bottom of the solar convective zone, and rising through the zone to the surface, respectively. It was found that the timescale of flux loss is  $\sim 1$  month, comparable to the rise time, and very much shorter than the solar cycle. Consequently, toroidal flux bundles cannot be stored inside the convective zone proper for extended periods of time and the layer of flux storage must have turbulent diffusivities (and therefore turbulent velocities) significantly lower than the convectively unstable layer. Flux loops rising through the convective zone lose a significant fraction of their magnetic flux during the rise.

While sunspots are far from being thin flux tubes, an application of our models to them still yields decay times comparable to those observed; besides, the linear area-lifetime relation is also returned. The inclusion of a moat flow with the observed velocities and perpendicular to the field lines however reduces the decay times to values incompatible with observations; thus, the moat flow may actually rather be more or less parallel to the field lines. Furthermore, turbulent erosion may explain the origin of the current sheet at the boundary of a sunspot. A curious feature of our model is that the decay rate does not only depend on the actual size of a spot but also on its original (i.e., maximal) size. This is the signature of a parabolic decay law only slightly departing from linear. Observations seem to confirm our prediction of a parabolic decay law (Petrovay & van Driel-Gesztelyi 1997). On the other hand, from the solutions obtained in this paper, we can estimate the Joule dissipation associated with the current sheet around a flux tube. Setting in the values corresponding to a sunspot, we obtain a photospheric power source that is 4 orders of magnitude lower than the solar radiative output on the corresponding area (an annulus of thickness  $1''$  around the spot), far too weak to be observed.

On the theoretical front, possible extensions of this work include a generalization by allowing the variation of physical quantities in the direction parallel to the tube, as well as tests of these results in three-dimensional MHD simulations.

The authors are grateful to Dr Manfred Schüssler for useful comments on this manuscript. This work was financed in part by the DGES project 95-0028 and by the OTKA under grant F012817.

## REFERENCES

- Barenblatt, G. I. 1983, in *Nonlinear Dynamics and Turbulence*, ed. G. I. Barenblatt, G. Iooss, & D. D. Joseph (Boston: Pitman), 48  
 Brickhouse, N. S., & LaBonte, B. J. 1988, *Sol. Phys.*, 115, 43  
 Caligari, P., Moreno-Insertis, F., & Schüssler, M. 1995, *ApJ*, 441, 886  
 Chan, K.-L., & Sofia, S. 1989, *ApJ*, 336, 1022  
 D'Silva, S., & Choudhuri, A. R. 1993, *A&A*, 272, 621  
 Fan, Y., Fisher, G. H., & McClymont, A. N. 1994, *ApJ*, 436, 907  
 Gnevishchev, M. N. 1938, *Pulkovo Obs. Circ.*, 24, 37  
 Gokhale, M. H., & Zwaan, C. 1972, *Sol. Phys.*, 26, 52  
 Gratton, J., & Minotti, F. 1990, *J. Fluid Mech.*, 210, 155  
 Jahn, K. 1989, *A&A*, 222, 264  
 Kim, Y.-C., Fox, P. A., Demarque, P., & Sofia, S. 1996, *ApJ*, 461, 499  
 Kitchatinov, L. L., Pipin, V. V., & Rüdiger, G. 1994, *Astron. Nachr.*, 315, 157  
 Lydon, T. J., Fox, P. A., & Sofia, S. 1992, *ApJ*, 397, 701  
 Martínez Pillet, V., Moreno-Insertis, F., & Vázquez, M. 1993, *A&A*, 274, 521  
 Moreno-Insertis, F. 1986, *A&A*, 166, 291  
 Moreno-Insertis, F., Schüssler, M., & Ferriz-Mas, A. 1992, *A&A*, 264, 686  
 Moreno-Insertis, F., & Vázquez, M. 1988, *A&A*, 205, 289  
 Pardon, L., Worden, S. P., & Schneeberger, T. J. 1979, *Sol. Phys.*, 63, 247  
 Petrovay, K., & van Driel-Gesztelyi, L. 1997, in *Advances in the Physics of Sunspots*, ed. B. Schmieder, J. C. del Toro Iniesta, & M. Vázquez (ASP Conf. Ser. 118; San Francisco: ASP), 145  
 Proctor, M. R. E., & Weiss, N. O. 1982, *Rep. Prog. Phys.*, 45, 1317  
 Rüdiger, G., & Kitchatinov, L. L. 1996, preprint  
 Sheeley, N. R., DeVore, C. R., & Boris, J. P. 1985, *Sol. Phys.*, 98, 219  
 Simon, G. W., & Leighton, R. B. 1964, *ApJ*, 140, 1120  
 Skumanich, A., Lites, B. W., & Martínez Pillet, V. 1994, in *Solar Surface Magnetism*, ed. R. J. Rutten & C. J. Schrijver (Dordrecht: Kluwer), 99  
 Spiegel, E. A., & Weiss, N. O. 1980, *Nature*, 287, 616  
 Sweet, P. A. 1950, *MNRAS*, 110, 69  
 Weiss, N. O. 1964, *Phil. Trans. R. Soc. A*, 256, 99  
 Zwaan, C. 1968, *ARA&A*, 6, 135